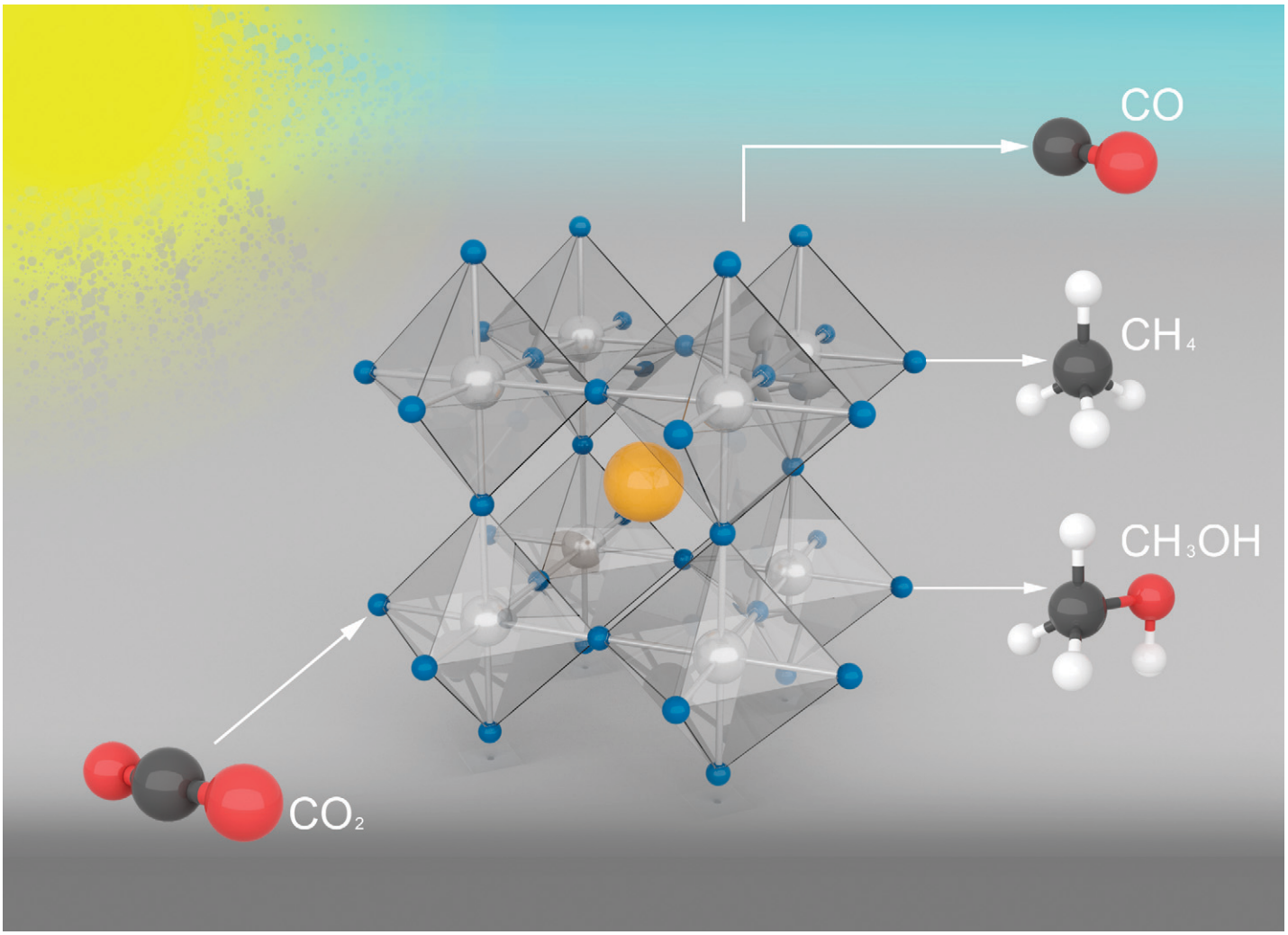

Showcasing research from Dr. Brenda Alcántar-Vázquez and Dr. Hugo A. Lara-García at Universidad Nacional Autónoma de México (UNAM), México.

Metal halide perovskites as an emergent catalyst for CO_2 photoreduction: a minireview

This minireview presents an overview of recent advances in CO_2 photoreduction using metal halide perovskites to support and encourage future research in this area. Different modifications to metal halide perovskites have been explored, such as heterojunction formation and the use of co-catalysts, resulting in better stability under polar solvents, charge separation, and longer carrier lifetime, leading to an enhanced photocatalytic reduction of CO_2.

As featured in:

See Brenda Alcántar-Vázquez, Hugo A. Lara-García *et al.*, *React. Chem. Eng.*, 2021, **6**, 828.

ROYAL SOCIETY OF CHEMISTRY

rsc.li/reaction-engineering

Registered charity number: 207890

Reaction Chemistry & Engineering

ROYAL SOCIETY OF CHEMISTRY

MINI REVIEW

View Article Online
View Journal | View Issue

Cite this: *React. Chem. Eng.*, 2021, **6**, 828

Metal halide perovskites as an emergent catalyst for CO_2 photoreduction: a minireview†

Melissa Méndez-Galván, [a] Brenda Alcántar-Vázquez, *[b] Gabriela Diaz, [a] Ilich A. Ibarra [c] and Hugo A. Lara-García *[a]

Received 26th January 2021,
Accepted 3rd March 2021

DOI: 10.1039/d1re00039j

rsc.li/reaction-engineering

Nowadays, the CO_2 conversion process is one of the most important technologies that must be promoted quickly. CO_2 photoreduction is, in the long term, a promising route to successfully reduce the CO_2 concentration. Searching for new strategies and efficient materials to enhance CO_2 photoreduction does not stop. Thus, metal halide perovskite materials have emerged as one of the leading candidates to achieve this goal due to their exceptional optoelectronic properties. This minireview presents an overview of recent advances in CO_2 photoreduction using metal halide perovskites to support and encourage future research in this area. The focus is on improving some optoelectronic properties to enhance photocatalytic activity through heterojunction formation and the use of co-catalysts.

Introduction

Global warming and climate change are two problems that have been studied since the last century. Despite that, the possible impact of these environmental problems is not fully known; one thing is clear: humanity is facing the first consequences concerning this crisis. Greenhouse gasses, among which CO_2 is one of the main in the atmosphere,[1] are responsible for increasing the Earth's temperature, melting ice at the poles, raising sea levels, and changing the seasons. Furthermore, humanity is running out of time to solve these environmental problems.[1,2]

There are four main routes to reduce the amount of CO_2 in the atmosphere: (i) decreasing the emission of CO_2; (ii) direct air capture and CO_2 capture at the point of source followed by underground/undersea storage; and (iii) CO_2 conversion. From these three methods, reducing the emission of CO_2 seems a utopian possibility, and the CO_2 capture and storage are strategies with increasing levels of technological readiness that bridge the gap towards implementation.[3] However, humans depend on carbon-based economies, so it is necessary to find solutions to achieve sustained population growth and improve global living standards. Therefore, there is a social, economic, and environmental incentive to use captured CO_2 as a carbon building unit. There are chemical, biological, thermochemical, electrochemical, photochemical, and photoelectrochemical techniques for the conversion of CO_2 into value-added chemicals and fuels.[4–8] Among these, CO_2 photoreduction is, in the long term, the most promising route to reduce atmospheric CO_2 concentrations.[3] The main advantages are that reduction products can be used as chemical fuels, and the process can be carried out by a photocatalytic system using sunlight.[9–11]

Additionally, the semiconductor should have essential characteristics to be considered a promising photocatalyst for CO_2 reduction: (i) the valence band must be more positive for the holes acting as an electron acceptor; (ii) the conduction band must be more negative than the CO_2 reduction potential; (iii) the adsorption capability of reactants into the photocatalyst surface should be high; (iv) the electron-pair recombination must occur in longer times than the chemical reaction; (v) no toxic by-product should be evolved during the photochemical reaction; (vi) the photocatalyst should have adequate stability, (vii) high surface area, (viii) resistance to photocorrosion, (ix) high adsorption of light in the visible range and (x) low cost.[12]

For many years, there has been a constant search for semiconductor materials that possess the best qualities for CO_2 photoreduction. In this search, probably the most studied photocatalyst has been TiO_2, alone, forming a heterostructure or nanoparticles on its surface (Cu, Au, Ag, Pt).[13–20] Nevertheless, TiO_2 only shows good activity under UV light irradiation

[a] *Instituto de Física, Universidad Nacional Autónoma de México, Apartado Postal 20-364, 0100, Ciudad de México, Mexico. E-mail: hugo.lara@fisica.unam.mx*
[b] *Instituto de Ingeniería, Coordinación de Ingeniería Ambiental, Universidad Nacional Autónoma de México, Circuito Escolar S/N, CU, Coyoacán, CP 04510, Ciudad de México, Mexico. E-mail: BAlcantarV@iingen.unam.mx*
[c] *Laboratorio de Fisicoquímica y Reactividad de Superficies (LaFReS), Instituto de Investigaciones en Materiales, Universidad Nacional Autónoma de México, 04510, Ciudad de México, Mexico*

† Electronic supplementary information (ESI) available: All the reaction parameters involved and the reaction product rates or yields of all the efforts made until now are summarized in Table S1. See DOI: 10.1039/d1re00039j

and suffers from surface charge recombination problems.[21] Thus, other semiconductors have been tested as photocatalysts such as ZnO,[22] ZrO_2,[23] perovskite oxides ABO_3,[24,25] BiOX (X = Br, Cl, and I),[26–28] g-C_4N_3,[29] and different metal–organic frameworks (MOFs).[30–40] Nonetheless, these photocatalysts have rapid recombination or inadequate band potential for oxidative and reductive reactions in CO_2 photoreduction or are active only under UV irradiation.

Perovskites have been widely explored in photovoltaic systems, light-emitting diodes, photodetectors, and lasers, among others, due to their unique photoelectrochemical properties and structural features, such as controllable particle size, reduced dimensionality, and adjustable chemical composition.[41–43] In the past decade, halide perovskites have emerged as one of the most promising materials for optoelectronic applications[44,45] since they combine ease of manufacture, low cost, and interesting semiconductor characteristics. These features include high absorption coefficient, high carrier diffusion, defect tolerance, efficient free charge-carrier generation, high photoluminescence quantum yield, narrow emission band, and tunable bandgap.[46,47] The halide perovskites possess a typical perovskite crystal structure of ABX_3, where A is an inorganic or organic cation, B a metal cation, and X a halide anion.[47] This structure provides the ability to perform a large number of atom replacements. This atom substitution offers an extensive amount of possible combinations of halide perovskites.[48,49] In recent years, the scientific community has focused its research on finding new perovskites suitable for optoelectronic applications. These efforts have produced astonishing results in this field.[44,47,50–53] Nevertheless, research has focused on applications such as solar cells, LEDs, and lasers. Halide perovskites have a vast and potentially attractive window for photocatalytic applications.[54,55] Compared to most conventional semiconductors, metal halide perovskites are relatively new as photocatalysts for CO_2 reduction. In the past year, some reviews have shown perovskite behavior in CO_2 photoreduction.[25,41,42] These recent spotlights confirm the great potential of these materials and the broad field of study that remains untapped. Some of these studies are not totally focused on metal halide perovskite or CO_2 photoreduction. They include the use of perovskite oxides[25] and metal halide perovskites in other photocatalytic reactions, such as the degradation of organic pollutants and organic synthesis.[41] Finally, Shyamal *et al.*[42] presented a halide perovskite perspective without classifying the modification strategies for enhancing the catalytic process. Here, the current minireview summarizes the recent progress of metal halide perovskites in photocatalytic CO_2 reduction, focusing on structure, heterojunctions, and their use of a co-catalyst to get an overview of the main strategies used to improve the photocatalytic process.

CO_2 photoreduction mechanism

Understanding the mechanism of CO_2 photoreduction is essential for developing a good photocatalyst. In general, a photocatalytic process occurs in three main steps: (i) absorption of light by a semiconductor and the simultaneous formation of charge carriers (electron–hole pairs); (ii) separation and migration of the charge carriers to the semiconductor surface; and (iii) the chemical reaction between the charge carriers and the chemical reactants. In this case, the third process implicates the CO_2 absorption, activation, and dissociation of the C–O bond.[56] The products coming from reducing the CO_2 molecule are partially reduced compounds (CO, HCOOH, HCHO, CH_3OH, and CH_4) (Fig. 1).[57,58]

CO_2 photoreduction is a complex reaction that involves multiple electrons that could lead to various products *via* different reaction pathways. Eqn (1)–(8) list half-equations to the several products commonly formed in CO_2 photoreduction in aqueous medium at a neutral pH.[59,60]

$$CO_2 + e^- \rightarrow CO_2^- - 1.90\ V \quad (1)$$

$$CO_2 + 2H^+ + 2e^- \rightarrow HCOOH - 0.61\ V \quad (2)$$

$$CO_2 + 2H^+ + 2e^- \rightarrow CO + H_2O - 0.53\ V \quad (3)$$

$$CO_2 + 4H^+ + 4e^- \rightarrow HCHO + H_2O - 0.48\ V \quad (4)$$

$$CO_2 + 6H^+ + 6e^- \rightarrow CH_3OH + H_2O - 0.38\ V \quad (5)$$

$$CO_2 + 8H^+ + 8e^- \rightarrow CH_4 + 2H_2O - 0.24\ V \quad (6)$$

$$2H_2O + 4h^+ \rightarrow O_2 + 4H^+\ 0.81\ V \quad (7)$$

$$2H^+ + 2e^- \rightarrow H_2 - 0.42\ V \quad (8)$$

As mentioned above, each product is formed by a different reaction pathway, making it difficult to understand the mechanism of the process fully. Some efforts have been made to understand the reaction mechanism; however, most of them are conducted in TiO_2 nanoparticles.[61] In addition, the

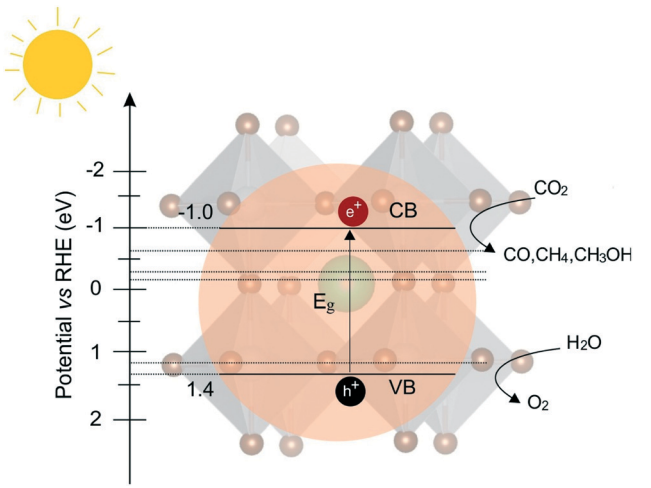

Fig. 1 Schematic representation of the CO_2 photoreduction process.

process can be affected by many factors such as the CO_2 adsorption mode, pH of the solution, surface functional groups, surface co-catalysts, temperature, photoreactor geometry, and pressure on surface diffusion, among others.

To date, most efforts to understand the mechanism of metal halide perovskite and thus design a better catalyst for CO_2 photoreduction have focused on light-harvesting, the generation, separation, and charge transportation, as shown below. The surface reactions deserve much more attention, particularly the adsorption and activation of CO_2 on the surface of catalysts because they play an important role in the efficiency and selectivity of the reaction.

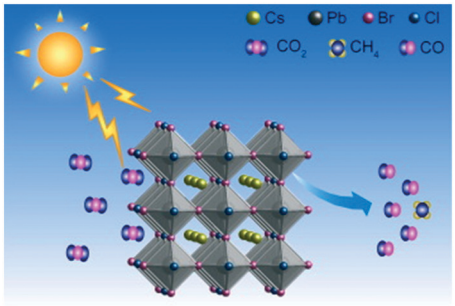

Fig. 2 Schematic representation of mixed halide perovskite (reprinted from ref. 44. Copyright 2019, with permission from Elsevier).

Halide perovskites

ABX_3 gives the crystal structure of halide perovskites. There are eight octahedra with the metal cation (B) in the center, forming the perovskites' ideal cubic structure. In the vertex of the octahedra are the halide anions (X = Cl, Br, or I); the octahedra can be rotated or tilted by replacing these anions. This change directly modifies the bandgap of the material.[62] The size of the B cation determines the formation of a close-packed perovskite structure because the B cation needs to fit in the four adjacent octahedra (BX_6), which are connected by corner-sharing.[63] The size of cation A is the key aspect for forming a close-packed perovskite structure.[64] In this typical perovskite configuration, the all-inorganic $CsPbX_3$ has become an emerging new optoelectronic material[65] and the photocatalytic application focus, particularly for CO_2 photoreduction due to its excellent semiconductor properties. This section reviews the strategies that have been studied to improve the performance of this semiconductor as a photocatalyst. Additionally, all the reaction parameters involved and the rates or yields of the reaction product of all the efforts carried out so far are summarized in Table S1 (ESI†).

In 2017, Hou *et al.*[66] studied the size effect in cesium lead halide perovskite for CO_2 photoreduction. In this work, a colloidal synthesis of $CsPbBr_3$ quantum dots (QDs, 3–12 nm) was reported. Some semiconductor properties such as bandgap energies and photoluminescence spectra are tunable over visible light spectra by quantum size effects. The results showed that the CO_2 reduction efficiency was deeply related to the perovskite size and the carrier lifetime, obviously. The 8.5 nm particles had the longest carrier lifetime. Furthermore, the use of quantum dots had a positive effect on selectivity, reaching over 99% with a yield rate of 20.9 μmol g^{-1} for CO (during 8 h of reaction).

The following year, Guo *et al.* reported[44] a strategy to increase the CO_2 photoreduction using mixed halide perovskites, $CsPb(Br_x/Cl_{1-x})_3$ (x = 0.7, 0.5, 0.3) (Fig. 2). The reaction was performed for nine hours under simulated sunlight. Mixed halide perovskites were shown to be an excellent photocatalyst, with great stability and selectivity for CO_2 conversion to CO and CH_4. The CsPb $(Br_{0.5}/Cl_{0.5})_3$ perovskite showed the best results, 875 μmol g^{-1} CO and 99% selectivity for CH_4, 4.5-, 9.1-, and 6-fold higher than that reported by $CsPbBr_3$, $CsPbCl_3$ and $CsPbI_3$, respectively, under the same conditions. These results were attributed to its more efficient charge separation capacity compared to the other mixed halide perovskites.

A theoretical study proposes that $CsPbBr_3$ doped with Fe and Co improves the reaction intermediates' adsorption, leading to methane as a favorable product.[67] Based on this, Syamal *et al.*[68] reported in 2019 CO_2 photoreduction using a cesium halide perovskite ($CsPbBr_3$) doped with Fe (3 wt%). Fe-doped $CsPbBr_3$ showed a better photoresponse compared to the undoped semiconductor. Under the same reaction conditions, enhancement of the photocatalytic activity and selectivity to CH_4 was achieved with the inclusion of Fe(II) instead of Pb(II) in the cesium lead halide perovskite. The experimental results of selectivity were in good agreement with that predicted by the theoretical results reported by Tang *et al.*[67] In 2020, Yu-Wei Liu *et al.* reported[69] the synthesis of a mixed halide perovskite doped with Mn (Mn-doped $CsPb(Br/Cl)_3$) and its photocatalytic reduction of CO_2. The photocatalytic reduction was improved when Mn-doped $CsPb(Br/Cl)_3$ was used compared to undoped perovskite. The Mn-doped perovskite with the highest CO_2 reduction was the one with a $PbBr_2$/MnCl ratio of 2 : 1. In this case, CO and CH_4 yields were 1917 and 82 μmol g^{-1}, 14.2 and 1.4 times higher, respectively, than that of the undoped perovskite. This sample presented higher UV-vis absorption, lower photoluminescence intensity, and a large photocurrent intensity.

Finally, Shyamal *et al.* recently studied the influence of facets and defects on CO_2 photoreduction (Fig. 3).[68] $CsPbBr_3$ nanostructures of high emission cubes, intermediate emission hexapod-shaped, and low emission non-cubic (polyhedral) were studied. The low photoluminescence quantum yield of non-cubic nanostructures was related to halide defects that act as a carrier trap. Additionally, the highest photocurrent density was achieved by non-cubic nanostructures, followed by hexapods and cubes. This same trend was found when the nanostructures were used as a photocatalyst for CO_2 reduction, where non-cubes were a better catalyst. A DFT study shows that the facets exposed by non-cubic nanostructures ({112} and {102}) have stronger CO_2 adsorption energies and lower CH_4 desorption energies compared to facets exposed by cubic nanostructures ({110} and {002}). Therefore,

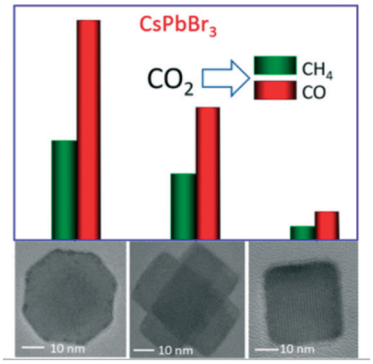

Fig. 3 Reaction product activity related to the morphology of $CsPbBr_3$ (reproduced with permission from ref. 68. Copyright 2020, American Chemical Society).

it is concluded that the existence of trap states helps to transfer the carriers that trigger the chemical reaction and the exposure of particular facets enhances the catalytic reaction.

From these results, it is clear that all-inorganic $CsPbX_3$ is an emerging and promising catalyst for CO_2 photoreduction under visible light. The main disadvantage is that lead halide perovskites are unstable under humid conditions, causing all photocatalytic experiments to be carried out using ethyl acetate as the oxidation solvent. CO_2 photoreduction is sensitive to quantum dot sizes, the facets exposed by the catalyst, the defects present in the semiconductor, and the halide cation's chemical composition. Furthermore, the photocatalytic activity and selectivity can be improved by doping the lead halide perovskite with transition metals such as Fe and Co or by mixing the halide ion content.

Halide double perovskites

Lead is the most widely used cation in metal halide perovskites; its use has allowed extraordinary optoelectronic applications. Nevertheless, the main problems with lead halide perovskites are toxicity and instability under ambient conditions. An alternative to address these problems[49,70] is to substitute two divalent lead ions with a monovalent ion and a trivalent metal ion. As a result of this substitution, the halide double perovskites, $A_2B'B''X_6$, were found.[71–73] In the same way, three divalent lead ions can be substituted by two trivalent metal ions to form a 0D family perovskites, $A_3B_2X_9$.[51,74,75] There are few reports in the literature on the performance of these perovskites in the photoreduction of CO_2.[51,72,75,76] However, the reported results highlight the good stability obtained under ambient conditions and the excellent optoelectronic properties of halide double perovskites for CO_2 reduction.[49]

In 2018, Zhou *et al.* reported[72] for the first time the synthesis of a lead-free double perovskite, $Cs_2AgBiBr_6$, and its activity for CO_2 photoreduction. Nanocubes with an average size of 9.5 nm are formed. Lead-free double perovskite was reported to be stable in a mild polar solvent for more than three weeks under light and humidity at 100 °C. $Cs_2AgBiBr_6$ nanocubes presented an indirect bandgap of 2.52 eV and a carrier lifetime of 7.5 ns. Likewise, after 6 hours of reaction under simulated sunlight and using ethyl acetate as the solvent, evolution of 14.1 μmol g^{-1} CO and 9.6 μmol g^{-1} CH_4 was achieved. A comparison with bulk $Cs_2AgBiBr_6$ was made, and the photocatalytic activity was found to be 18 times less than that of nanocubes, suggesting that nanocubes improved catalytic performance. Therefore, $Cs_2AgBiBr_6$ nanocubes have an adequate conduction band for CO_2 photoreduction (Fig. 4).

In 2019, Bhosale *et al.* investigated[51] a lead-free 0D family perovskite, $A_3Bi_2I_9$ ($A = Rb^+$, Cs^+, and MA^+), for CO_2 reduction obtained by a new top-down synthesis method *via* ultrasonication. In the photoreduction reaction, a reaction time of 10 hours was reported under UV light irradiation, quantifying CO and CH_4 as reaction products, and TiO_2 (P25) was used as a reference photocatalyst. All perovskites showed better catalytic activity than TiO_2, and the CO production trend was $Cs_3Bi_2I_9 > Rb_3Bi_2I_9 > MA_3Bi_2I_9$ and for CH_4 $Rb_3Bi_2I_9 > Cs_3Bi_2i_9 > MA_3Bi_2I_9$. DRIFT experiments give an insight into the plausible mechanism of CO_2 photoreduction. Also, stability tests for lead-free perovskites show that bismuth-based perovskites, $A_3Bi_2I_9$, are stable for seven days in humid and light conditions.

Lu *et al.* reported[75] an Sb-based perovskite, $Cs_3Sb_2Br_9$. $Cs_3Sb_2Br_9$ presented a 2.64 eV bandgap, which is active under visible light irradiation. Photocatalytic CO_2 reduction was tested by measuring CO as a product. A comparison between the CO production rate of $Cs_3Sb_2Br_9$ and $CsPbBr_3$ shows that after four hours of reaction, the CO production was 50 and 510 μmol g^{-1} for $CsPbBr_3$ and $Cs_3Sb_2Br_9$, respectively, that is, ten times larger for the lead-free halide perovskite. DFT

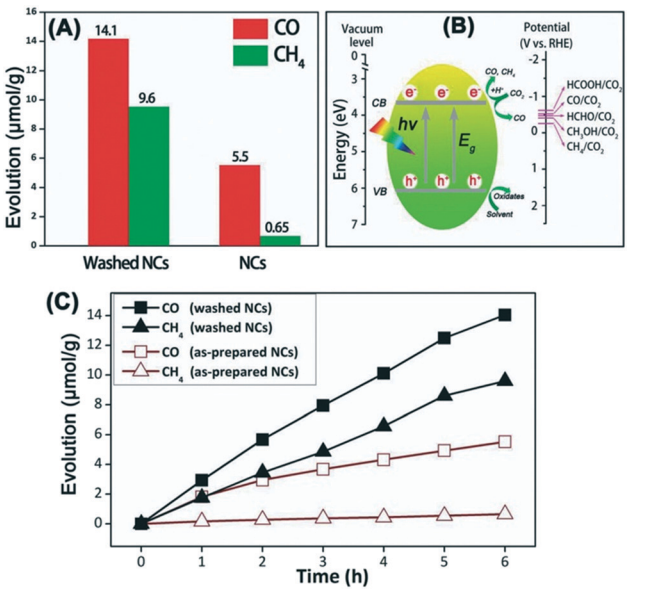

Fig. 4 Comparison of photocatalytic performance between as-prepared and washed $Cs_2AgBiBr_6$ (A), schematic diagram of the CO_2 photoreduction (B), and evolution of products over time (C) (reproduced with permission from ref. 72. Copyright 2018, John Wiley and Sons).

analysis shows many intermediate binding sites (COOH and CO*) on the surface ((1000) and (0001)) of $Cs_3Sb_2Br_9$, which may be the key to the enhancement of activity. Furthermore, stability tests showed that lead-free perovskite remains stable after 9 hours of reaction, an advantage over lead perovskite instability. Finally, in 2020, Sheng *et al.*[76] studied a lead-free halide perovskite $Cs_3Bi_2X_9$ (X = Cl, Br, I). The $Cs_3Bi_2Br_9$ had better efficiency and selectivity compared to $Cs_3Bi_2Cl_9$ and $Cs_3Bi_2I_9$. Theoretical and experimental results demonstrated that Br could effectively narrow the bandgap, inhibit charge carrier recombination, and promote directional electron delivery. More importantly, the active site associated with Br on the surface can alter the adsorption and activation modes of CO_2 on the surface of the perovskites, leading to better catalytic performance.

The use of halide double perovskites, $A_2B'B''X_6$, and halide perovskites with three divalent metal ions, $A_3B_2X_9$, as lead-free perovskites, turns out to be a promising way to decrease toxicity and improve stability without diminishing the capacity of CO_2 photoreduction.

Halide perovskites in heterojunctions

It is often difficult for a perovskite, as a single-component, to meet all the requirements of a high-efficiency photocatalyst simultaneously. Some critical problems need to be solved: a) the poor stability toward the moisture, polar solvents, or high temperature, b) agglomeration, and c) high electron–hole recombination.[41] Among the strategies to solve these problems and improve the activity of halide perovskites for CO_2 photoreduction, the construction of a heterojunction has aroused growing interest.[77–79] A heterojunction is the coupling of two semiconductors that allows overcoming the main downsides of typical photocatalysts: the limited absorption of visible light and the fast recombination of electron–hole pairs.[80,81] In this section, the efforts that various research groups have made to construct an effective heterojunction using metal halide perovskites are brought together.[9,50,77,82–85]

Metal–organic frameworks (MOFs) are porous hybrid materials that are recently emerging as new types of photoactive materials for CO_2 reduction due to their excellent CO_2 adsorption capability and unique structural characteristics. However, MOFs suffer from fast electron–hole recombination after light excitation.[86] In this regard, several attempts have been made to improve the photocatalytic activity by forming a heterojunction between MOFs and metal halide perovskites.

In 2018, Kong *et al.*[77] reported the synthesis of a heterojunction formed by $CsPbBr_3$ and two different cobalt-based MOFs (ZIF-8 and ZIF-67) in a core@shell structure. The core@shell heterojunction was prepared by an *in situ* synthesis process dispersing presynthesized $CsPbBr_3$ QDs into the precursor solution of a metal ion and imidazole ligand. The heterojunction showed a synergetic ability for CO_2 photoreduction; the electron consumption rate for $CsPbBr_3$@ZIF-8 and $CsPbBr_3$@ZIF-67 was 15.498 and 29.630 μmol g^{-1} h^{-1}, respectively, 1.39 and 2.66 times more than with $CsPbBr_3$. Likewise, the heterostructure showed stability during six cycles of use under visible light. The enhancement in catalytic performance was attributed to the improvement in charge separation efficiency and Co centers in MOFs that adsorb and activate CO_2 molecules (Fig. 5).

Additionally, Wan *et al.*[85] investigated the heterostructure catalytic performance built by $CsPbBr_3$ QDs and UiO-66(NH_2). The nanocomposite was synthesized by an ultrasonic hybrid approach, varying the halide perovskite amount in the system (0, 5, 10, 15, 30 wt%). The photocatalytic reduction of CO_2 was carried out in water and ethyl acetate under visible light. Compared to the pristine systems, the heterostructure showed a better CO production rate with the optimum load of 15 wt% $CsPbBr_3$ QDs, and a CO production rate of 98.57 μmol g^{-1} h^{-1}. The photocatalytic activity improvement was attributed to the separation and transfer of electrons at the interface between $CsPbBr_3$ QDs and UiO-66(NH_2). Wu *et al.*[87] studied a heterojunction made up of encapsulated QDs of $CH_3NH_3PbI_3$ ($MAPbI_3$) in the pores of Fe-porphyrin-based MOFs of PCN-221(Fe_x). It was demonstrated that the photogenerated electrons in the $MAPbI_3$ QDs could be transferred to the Fe catalytic sites, achieving an efficient charge separation that results in better CO_2 conversion, 38 times higher than the pristine MOFs. Cheng *et al.*[88] reported a heterojunction between MIL-100 (Fe) and $CsPbBr_3$ synthesized in water resulting in two different perovskite structures in the heterojunction, $CsPbBr_3$ and $CsPbBr_5$. The heterostructure with 18 wt% MIL-100 (Fe) showed the highest CO production rate of 20.4 μmol g^{-1} h^{-1}, 4.5 times more than the parts that conform to the heterojunction. The increase in activity was attributed to the proper match between the bands of $CsPbBr_3$ and MIL-100 (Fe), which causes the electron transfer between conduction bands. All these results showed that heterojunctions between MOFs and metal halide perovskites could improve stability, enhance CO_2 adsorption and activation in MOF metallic centers, and facilitate charge transfer between each semiconductor by inhibiting charge recombination.

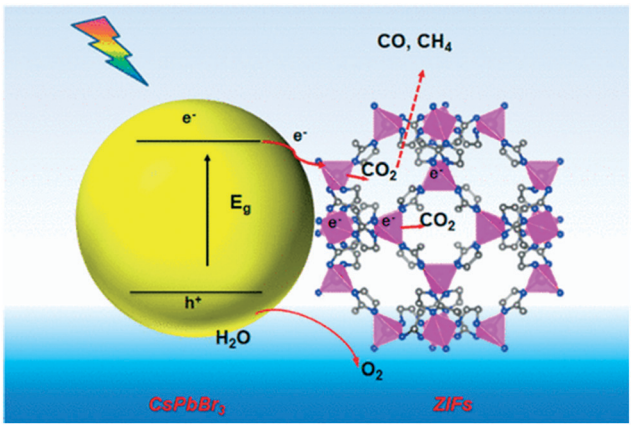

Fig. 5 Schematic illustration of the charge transfer and CO_2 photoreduction process of $CsPbBr_3$/ZIFs. (Reproduced with permission from ref. 77. Copyright 2018, American Chemical Society).

This year Wang *et al.*[89] reported a heterojunction between $CsPbBr_3$ and covalent triazane frameworks (CFTs) for visible-light-driven CO_2 reduction. The addition of CFTs enhances the CO_2 adsorption/activation capacity. Additionally, the energy band structures of $CsPbBr_3$ and CFT allow the charge transfer, facilitating the charge separation. As a result, the heterojunction shows a superior photocatalytic activity towards CO_2 reduction, being 5 and 4 times higher than $CsPbBr_3$ and CFT, respectively.

Another type of heterojunction is that formed by two different metal halide perovskites. Mu *et al.*[90] studied a heterojunction of cobalt-doped $CsPbBr_3$–Cs_4PbBr_6. The addition of cobalt (0.5–3%) did not change the composite bandgap value but promoted charge transfer and separation of photogenerated carriers, prolonging the lifetime and improving CO_2 photocatalytic conversion. The main advantage was that the photocatalytic reactions were carried out using water as the solvent (first report). Later, the use of methanol (an oxidizing organic substrate) and a heterojunction of $CsPbBr_3$ embedded in a matrix of Cs_4PbBr_6 and doped with Co was reported by Dong *et al.*[91] Methanol accelerates the rate of hole consumption and improves the reduction of CO_2 to CO. The maximum photoreduction yield, after 15 hours, for the heterojunction Co1%@$CsPbBr_3$/Cs_4PbBr_6 was 1835 μmol g^{-1}. The main advantage of this heterojunction is the stability of the composite in a polar solvent compared to pure $CsPbBr_3$.

Due to the promising results, $CsPbBr_3$ heterojunctions continued to be studied to reduce charge recombination. In the heterojunction of $CsPbBr_3$ immobilized on 2D black phosphorus (BP) (Fig. 6), the BP enhances charge separation by trapping photoexcited electrons from $CsPbBr_3$ and generates active sites for CO_2 activation. As a result, a 2.4- and 4.4-fold improvement in the yield of CH_4 and CO products was observed compared to unmodified lead-halide perovskite.[50] The catalytic activity remains almost stable after ten CO_2 photoreduction cycles. The charge recombination was reduced, and the carrier lifetime was extended in the heterojunction of $CsPbBr_3$ quantum dots (CPB) and porous g-C_3N_4 (PCN) by creating an N–Br bond.[83] The bandgap energy values were 2.64 (PCN) and 2.18 eV (CPB); therefore the bands' alignment can induce photoexcited electrons and holes by the offset of conduction and valence bands. The 20 wt% CPB-PCN photocatalyst exhibits an outstanding performance of 149 μmol g^{-1} h^{-1} for photocatalytic reduction of

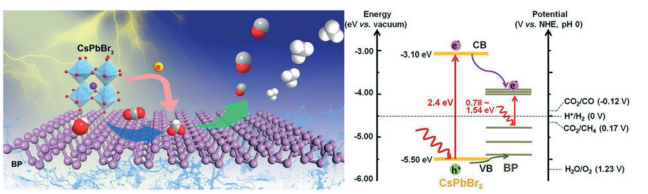

Fig. 6 $CsPbBr_3$/BP scheme for photocatalytic CO_2 reduction under light irradiation and its band diagrams (adapted from ref. 50. Copyright 2020, with permission from Elsevier).

CO_2 to CO, which is 15 times higher than that of pristine CPB quantum dots. Similar work was reported by Cheng *et al.*,[82] who obtained a heterojunction between $CsPbX(Br_x$-$Cl_{1-x})$/g-C_3N_4 by *in situ* solvothermal synthesis. The CO production was five times higher than that in the pure constituents. As in the previous case, the results were mainly attributed to an efficient charge separation due to a proper match between the band structure of $CsPbBr_3$ and g-C_3N_4. A heterojunction of $CsPbBr_3$ immobilized on monolayer MoS_2 nanosheets ($CsPbBr_3$/MoS_2) was reported by Wang *et al.*[92] The photoreduction was carried out in a solution of ethyl acetate and water. Compared to pure $CsPbBr_3$, the heterojunction $CsPbBr_3$/MoS_2 achieved a 3.0- and 2.4-fold conversion of CO_2 to CH_4 and CO, respectively. Like other heterojunctions, increased charge separation generates more active sites to facilitate CO_2 activation, thereby increasing the activity.

Guo *et al.*[93] studied the functionalization of a heterojunction formed by $CsPbBr_3$ nanocrystals with graphitic carbon nitride, containing titanium oxide species (TiO–CN), $CsPbBr_3$@TiO–CN, using water as the electron source. The introduction of TiO–CN into the heterostructure led to an increased number of active sites boosting the charge separation between $CsPbBr_3$ and TiO–CN. After ten hours of irradiation, the heterostructure produced six and three times more CO than TiO–CN and $CsPbBr_3$, respectively, reflecting the advantage of a heterojunction over pristine materials. Finally, Jiang *et al.*[79] reported a heterostructure formed by $CsPbBr_3$ nanocrystals anchored on a branched ZnO nanowire/3D macroporous graphene oxide scaffold (MRGO). The results obtained for CO_2 photoreduction reveal a synergic effect between 0D $CsPbBr_3$ NC, 1D ZnO NW and 3D MRGO. Highlighting the improvement of visible light absorption and the selectivity of CH_4, which remains with the minimum change, during four reuse cycles. The higher selectivity of CH_4 could be attributed to the enriched electrons on the MRGO, which facilitate the reaction of CO_2 absorbed molecules on the surface.

Additionally, Z-scheme heterojunctions have been studied using $CsPbBr_3$ perovskite. The Z-scheme heterojunction can realize the spatial separation of photoinduced charges and ensure strong redox capability simultaneously.[94–96] Wang *et al.*[84] announced a heterojunction in a direct Z-scheme made up of quantum dots of $CsPbBr_3$ on Bi_2WO_6 nanosheets (Fig. 7). A 9.5-fold improvement in CO production was achieved with a 1 : 5 mass ratio $CsPbBr_3$: Bi_2WO_6 heterostructure compared to pristine $CsPbBr_3$. The photocatalytic activity improvement was related to efficient charge separation and preservation of the high reduction potential on the $CsPbBr_3$ side. Unlike the $CsPbBr_3$ quantum dots, the heterojunction remains stable after four cycles of photocatalysis. Jiang *et al.*[78] reported a heterojunction Z-scheme composed of α-FeO_3/amine-RGO/$CsPbBr_3$. In CO_2 photoreduction experiments, methane was found as the main product, with a total yield in the Z-scheme of 181.68 μmol g^{-1}, higher than that obtained with α-FeO_3/$CsPbBr_3$ (66.64 μmol g^{-1}) and pristine

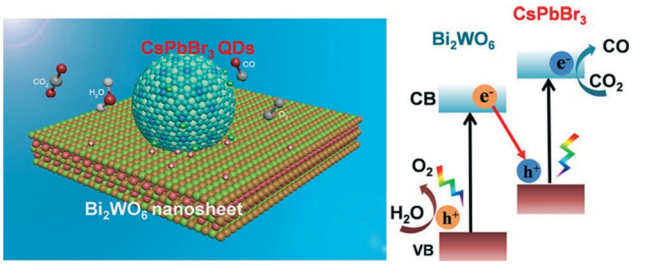

Fig. 7 Z-scheme of a photocatalytic system for CO_2 reduction and possible charge carrier scheme (adapted with permission from ref. 84. Copyright (2020), American Chemical Society).

$CsPbBr_3$ (30.55 μmol g^{-1}). The addition of amine-RGO leads to greater charge separation and prolongs carrier lifetime. Comparing these two reports, $CsPbBr_3$:Bi_2WO_6 exhibits a better electron production rate ($R_{electron}$ = $2R(CO) + 8R(CH_4)$) than α-FeO_3/amine-RGO/$CsPbBr_3$, 114.4 and 80.9 μmol g^{-1} h^{-1}, respectively.

Another *Z* scheme reported recently was the one by Mu *et al.*[97] The scheme was constructed using $CsPbBr_3$, α-Fe_2O_3, and ultrathin and small-sized graphene oxide (USGO) nanosheets as the electron mediator. The photocatalytic CO_2 reduction was carried out under visible light in a CO_2 saturated acetonitrile/water solution under simulated sunlight irradiation with CO as the principal product. The yield of production was 3.7 μmol g^{-1} h^{-1} for $CsPbBr_3$, 0.0 μmol g^{-1} h^{-1} for α-Fe_2O_3, 5.8 μmol g^{-1} h^{-1} for $CsPbBr_3$/α-Fe_2O_3, 14.6 μmol g^{-1} h^{-1} for $CsPbBr_3$/USGO and 73.8 μmol g^{-1} h^{-1} for $CsPbBr_3$/USGO/α-Fe_2O_3 which represents nineteen times more than that of pure $CsPbBr_3$. The Z-scheme behavior in the reuse cycles shows an activity that remains at 90%, indicating the stability of this scheme. These results can be attributed to the easy coupling between $CsPbBr_3$ and α-Fe_2O_3 with USGO nanosheets that allow a strong chemical bond and an enhancement in the charge separation between $CsPbBr_3$ and α-Fe_2O_3.

Finally, Xu *et al.*[98] reported in an experimental–theoretical study a Z-scheme made up of TiO_2/$CsPbBr_3$ quantum dots, synthesized by an electrostatic-driven self-assembling approach. The photocatalytic CO_2 reduction was carried out in an acetonitrile/water matrix and under a xenon lamp. The CO production yields in an hour were 6.6, 7.97, 11.45, 13.49, 11.33, 9.85, 6.2 μmol g^{-1} for TiO_2, TiO_2/0.5$CsPbBr_3$, TiO_2/1$CsPbBr_3$, TiO_2/2$CsPbBr_3$, TiO_2/3$CsPbBr_3$, TiO_2/4$CsPbBr_3$, and $CsPbBr_3$, respectively. These results are attributed to the electron transfer in the internal field, which drives the photoexcited electrons from TiO_2 to $CsPbBr_3$, providing more efficient electron–hole separation and thus more efficient CO_2 photoreduction.

Therefore, forming a heterojunction through the use of halide perovskites represents a new alternative, making it possible to design a photocatalyst in which the best qualities of each part that constitute the heterojunction are assembled. This may result in improving the stability of lead halide perovskites under polar solvents such as methanol or water. Also, proper band alignment may improve charge separation and extend the lifetime of the carriers, resulting in enhanced photocatalytic activity.

Halide perovskites as a co-catalyst

One of the most studied strategies to enhance the activity and selectivity of CO_2 photoreduction is using different kinds of co-catalysts.[99,100] This section summarizes the coupling of halide perovskites with a co-catalyst.

In 2017 Xu *et al.*[9] reported for the first time the use of a composite formed by $CsPbBr_3$ and graphene oxide (GO) for artificial photosynthesis (Fig. 8). In this work, the ability of CO_2 photoreduction by pristine material, $CsPbBr_3$ QDs, and the composite $CsPbBr_3$ QDs/GO, was studied. An enhancement in photocatalytic activity was reported when the composite was used compared to that obtained using pristine material; the rate of electron consumption improved from 23.7 to 29.8 μmol g^{-1} h^{-1} after the addition of GO. The increase in photocatalytic activity was attributed to GO electron-extraction ability. The GO Fermi level is more positive than the edge of the $CsPbBr_3$ conduction band, allowing the transfer of electrons from the semiconductor to the graphene oxide. In the same way, Pan *et al.*[101] reported $CsPbBr_3$ nanocomposites supported on MXene nanosheets (an emergent 2D material). A quenching in the photoluminescence quantum yield efficiency, shorter photoluminescence decay life and an improvement in photocurrent experiments suggest efficient charge transfer between the $CsPbBr_3$ and MXene nanosheets, leading to an enhancement in photocatalytic activity for the selective reduction of CO_2 to CO and CH_4 compared to pristine $CsPbBr_3$. As in the previous case, the excellent charge transfer is because of the Fermi level of MXene being more positive than the edge of the $CsPbBr_3$ conduction band.

Recently, in 2020, Chen *et al.*[102] reported on the construction of a hybrid photocatalytic system, $CsPbBr_3$-Ni(tpy), through electrostatic interactions and its behavior in CO_2 reduction. The results exhibit a high yield, 1724 μmol g^{-1}, of CO and CH_4, approximately 26-fold higher compared to $CsPbBr_3$ perovskite. The Ni(tpy) immobilization on $CsPbBr_3$

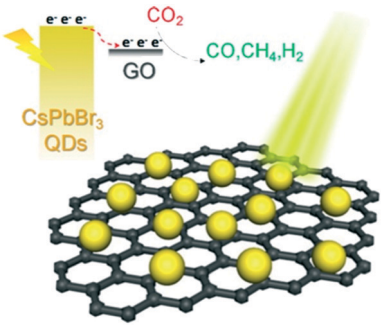

Fig. 8 CO_2 photoreduction diagram over $CsPbBr_3$ QD/GO (reproduced with permission from ref. 9. Copyright 2017, American Chemical Society).

facilitates the transfer of electrons from cesium halide perovskite to Ni(tpy) catalytic centers. Electron transfer was corroborated by quenching in photoluminescence and improvement in photocurrent experiments.

Another strategy to enhance photocatalytic activity is metal and metal nanoparticles coupled with a metal halide perovskite. In this sense, in 2018, Xu *et al.*[103] investigated a novel system composed of zero-dimensional $CsPbBr_3$ nanocrystals ($CsPbBr_3$ NCs) and two-dimensional Pd nanosheet (Pd NS). The CO_2 photoreduction was reported in the presence of H_2O vapor under visible light illumination. The highest electron consumption rate found was 33.79 μmol g^{-1} h^{-1}, corresponding with the material synthesized with 600 μL of Pd NS colloid solution. This yield of electron consumption is 2.43 times the yield of the pristine material. The increment in the photoreduction of CO_2 was related to the formation of a metal/semiconductor Schottky barrier that helps to accelerate the charge separation and transfer. Pd NS acts as an electron reservoir for a quicker separation of the electron–hole pair in $CsPbBr_3$ NC. Chen *et al.*[104] reported a system integrated by Pt nanoparticles on the $CsPbBr_3$ surface. Results show that with the addition of 0.79 wt% Pt (nanoparticles of 3–7 nm) on the $CsPbBr_3$ surface, the H_2, CO, and CH_4 production rates increase by 307.7, 102, and 94.4%, respectively. However, a decrease in CO_2 selectivity was reported, from 95.2 to 90.56%. The creation of a Schottky barrier (metal–semiconductor) can enhance the CO_2 activation and delay electron–hole recombination. Finally, Liao *et al.*[100] reported, for the first time, a plasmonic nanocomposite of $CsPbBr_3$–Au for the photocatalytic reduction of CO_2 (Fig. 9). Under visible light, CO and CH_4 production yields increase 3.2 times for $CsPbBr_3$–Au compared to the $CsPbBr_3$ perovskite. This improvement is explained by a transfer of electrons from the conduction band of $CsPbBr_3$ to Au (λ >420) and a transfer of plasmonic electrons from Au to $CsPbBr_3$ (λ > 580 nm). In addition, the coupling of plasmonic Au with $CsPbBr_3$ broadens the absorption region and enhances charge separation efficiency. Therefore, the use of noble metal nanoparticles can improve catalytic activity by creating a Schottky barrier or by plasmonic effects.

The use of a co-catalyst with metal halide perovskites represents a novel and effective strategy to improve the response of perovskites in CO_2 photoreduction by enhancing mainly the charge transfer.

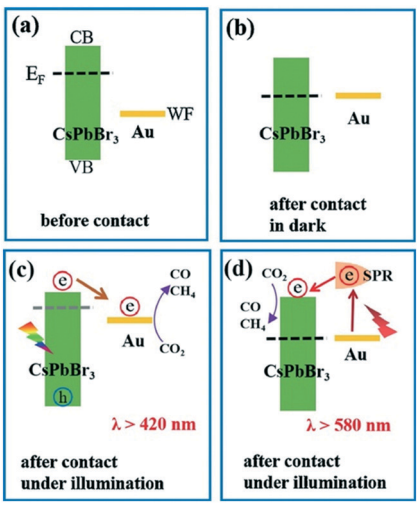

Fig. 9 Band structure of $CsPbBr_3$ nanocrystal and Au nanoparticle (a) before contact, (b) Fermi level alignment after close contact in the dark. Schematic diagram of excitation wavelength-dependent two charge separation mechanisms in $CsPbBr_3$–Au nanocomposite (c) under light irradiation with λ >420 nm and (d) under λ >580 nm (reprinted from ref. 100. Copyright 2021, with permission from Elsevier).

Challenges and outlook of the CO_2 photoreduction technology

Currently, the implementation of the CO_2 photoreduction process using metal halide perovskites as photocatalysts maintains several process limitations. Most research focuses on increasing the efficiency and extending the charge carrier lifetime, but this is not the complete picture of the process. After exposure to air, moisture, or UV light, the structure and photophysical properties of halide perovskite materials deteriorate significantly.[42] In addition, the function of water is well known in the CO_2 photoreduction process; nevertheless, as most of the perovskites under study are unstable in polar solvents, other solvents have been used (ethyl acetate, octadecene, trichloroethane, acetonitrile, and toluene), and the effect of each solvent in the process mechanism has not been deeply studied.

In the past four years, research has focused on the lead metal halide perovskite $CsPbBr_3$. This material has outstanding optoelectronic properties; however, its instability under polar solvents and its toxicity (lead) make it almost impossible to implement this technology. To face these disadvantages, researchers have to explore other alternatives such as lead-free metal halide perovskite. In recent years several researchers investigated these new materials for other applications such as solar cells with remarkable results.[70,105] This brings a broad spectrum of new metal halide perovskites that are unexplored as photocatalysts.

Additionally, it is well known that electron donors and hole scavengers play a prominent role in photocatalytic activity for CO_2 reduction.[106] In particular, the use of organic and inorganic hole scavenging is completely uninvestigated in metal-halide perovskite-based photocatalysts.

Other critical issues have to be addressed to successfully scale the CO_2 photoreduction. One of the most challenging tasks is comparing and selecting optimal photocatalysts because of the considerable variation in experimental setups, protocols, and photoreactor designs. Process parameters such as temperature and pressure on surface diffusion, photocatalyst degradation, the impact of light absorption, photoreactor geometry, and photocatalyst distribution on the photons' spatial distribution must be studied carefully. Another aspect that has not been addressed so far is the development

of CO_2 photoreduction kinetics. Extrinsic kinetic models such as Langmuir and Hinshelwood, dependent on the scale used, photoreactor geometry, and light transport, have been used. Nevertheless, intrinsic kinetic models independent of the photoreactor geometry are critical for scaling CO_2 photoreduction as they offer an opportunity to develop photoreactor design.[60] Finally, although little addressed, one of the fundamental challenges is measuring the change of CO_2 concentration during the process. Published studies mostly focus on CH_4 and CO production (Table S1†), so a full mass balance is not being considered.

Conclusions

The CO_2 photoreduction process is a potential technology for CO_2 conversion, and most efforts have focused on photocatalyst development. In this sense, metal halide perovskites have emerged as one of the most potential and promising materials for CO_2 photoreduction under visible light. Nevertheless, these materials face two principal disadvantages: instability in polar solvents and toxicity in the lead halide perovskite. Instead of representing problems, these disadvantages offer an opportunity to work out new strategies to develop and improve materials that can enhance the photocatalytic reduction of CO_2 under visible light. To deal with these disadvantages, doping halide perovskites, ABX_3, the use of halide double perovskites, $A_2B'B''X_6$, and halide perovskites with three divalent metal ions, $A_3B_2X_9$, the configuration of a heterojunction and the use of a co-catalyst, are proposed. All these new alternatives for metal halide perovskites have improved the stability under polar solvents, enhanced the charge separation, and prolonged the carrier's lifetime, which result in an enhancement in the photocatalytic CO_2 reduction.

Therefore, the incredible number of possible combinations and modifications of metal halide perovskites brings a broad spectrum for research in which it is possible to create, modify, improve, and finally enhance the photocatalytic activity to reduce the CO_2 atmospheric concentrations. Some challenges must be addressed to develop this technology further, such as identifying and quantifying the other reaction products, the influence of the process parameters, and kinetics.

Conflicts of interest

There are no conflicts to declare.

Acknowledgements

Melissa Méndez-Galván thanks the scholarship financial support of PNPC-CONACyT. Hugo A. Lara-García acknowledges the project PAPIIT-UNAM (IA103621) for financial support.

Notes and references

1 J. He and C. Janáky, *ACS Energy Lett.*, 2020, **5**, 1996–2014.
2 K. Li, B. Peng and T. Peng, *ACS Catal.*, 2016, **6**, 7485–7527.
3 H. Wu, X. Li, C. Tung and L. Wu, *Adv. Mater.*, 2019, **31**, 1900709.
4 S. Sultana, P. Chandra Sahoo, S. Martha and K. Parida, *RSC Adv.*, 2016, **6**, 44170–44194.
5 C. Costentin, J. C. Canales, B. Haddou and J. M. Savéant, *J. Am. Chem. Soc.*, 2013, **135**, 17671–17674.
6 A. J. Martín, G. O. Larrazábal and J. Pérez-Ramírez, *Green Chem.*, 2015, **17**, 5114–5130.
7 J. L. White, M. F. Baruch, J. E. Pander, Y. Hu, I. C. Fortmeyer, J. E. Park, T. Zhang, K. Liao, J. Gu, Y. Yan, T. W. Shaw, E. Abelev and A. B. Bocarsly, *Chem. Rev.*, 2015, **115**, 12888–12935.
8 O. Ola and M. M. Maroto-Valer, *J. Photochem. Photobiol., C*, 2015, **24**, 16–42.
9 Y. F. Xu, M. Z. Yang, B. X. Chen, X. D. Wang, H. Y. Chen, D. Bin Kuang and C. Y. Su, *J. Am. Chem. Soc.*, 2017, **139**, 5660–5663.
10 J. K. Stolarczyk, S. Bhattacharyya, L. Polavarapu and J. Feldmann, *ACS Catal.*, 2018, **8**, 3602–3635.
11 G. Zhao, X. Huang, X. Wang and X. Wang, *J. Mater. Chem. A*, 2017, **5**, 21625–21649.
12 S. C. Shit, I. Shown, R. Paul, K.-H. Chen, J. Mondal and L.-C. Chen, *Nanoscale*, 2020, **12**, 23301–23332.
13 R. Nematollahi, C. Ghotbi, F. Khorasheh and A. Larimi, *J. CO_2 Util.*, 2020, **41**, 101289.
14 W.-J. Ong, M. M. Gui, S.-P. Chai and A. R. Mohamed, *RSC Adv.*, 2013, **3**, 4505.
15 L. Liu, Y. Jiang, H. Zhao, J. Chen, J. Cheng, K. Yang and Y. Li, *ACS Catal.*, 2016, **6**, 1097–1108.
16 X. Meng, S. Ouyang, T. Kako, P. Li, Q. Yu, T. Wang and J. Ye, *Chem. Commun.*, 2014, **50**, 11517–11519.
17 M. Tahir, B. Tahir and N. A. S. Amin, *Appl. Catal., B*, 2017, **204**, 548–560.
18 A. Crake, K. C. Christoforidis, R. Godin, B. Moss, A. Kafizas, S. Zafeiratos, J. R. Durrant and C. Petit, *Appl. Catal., B*, 2019, **242**, 369–378.
19 W. A. Thompson, A. Olivo, D. Zanardo, G. Cruciani, F. Menegazzo, M. Signoretto and M. M. Maroto-Valer, *RSC Adv.*, 2019, **9**, 21660–21666.
20 G. Yang, D. Chen, H. Ding, J. Feng, J. Z. Zhang, Y. Zhu, S. Hamid and D. W. Bahnemann, *Appl. Catal., B*, 2017, **219**, 611–618.
21 N. Shehzad, M. Tahir, K. Johari, T. Murugesan and M. Hussain, *J. CO_2 Util.*, 2018, **26**, 98–122.
22 P. Li, H. Hu, G. Luo, S. Zhu, L. Guo, P. Qu, Q. Shen and T. He, *ACS Appl. Mater. Interfaces*, 2020, **12**, 56039–56048.
23 X. Wang, L. Zhang, H. Lin, Q. Nong, Y. Wu, T. Wu and Y. He, *RSC Adv.*, 2014, **4**, 40029–40035.
24 S. Zeng, P. Kar, U. K. Thakur and K. Shankar, *Nanotechnology*, 2018, **29**, 052001.
25 Y. W. Teh, M. K. T. Chee, X. Y. Kong, S.-T. Yong and S.-P. Chai, *Sustainable Energy Fuels*, 2020, **4**, 973–984.
26 D. Wu, L. Ye, H. Y. Yip and P. K. Wong, *Catal. Sci. Technol.*, 2017, **7**, 265–271.
27 J. C. Wang, H. C. Yao, Z. Y. Fan, L. Zhang, J. S. Wang, S. Q. Zang and Z. J. Li, *ACS Appl. Mater. Interfaces*, 2016, **8**, 3765–3775.

28 J. Jin, Y. Wang and T. He, *RSC Adv.*, 2015, **5**, 100244–100250.
29 S. Ye, R. Wang, M.-Z. Wu and Y.-P. Yuan, *Appl. Surf. Sci.*, 2015, **358**, 15–27.
30 I. I. Alkhatib, C. Garlisi, M. Pagliaro, K. Al-Ali and G. Palmisano, *Catal. Today*, 2020, **340**, 209–224.
31 S. Wang, J. Lin and X. Wang, *Phys. Chem. Chem. Phys.*, 2014, **16**, 14656.
32 S. Wang, B. Y. Guan and X. W. D. Lou, *J. Am. Chem. Soc.*, 2018, **140**, 5037–5040.
33 H. Zhao, X. Wang, J. Feng, Y. Chen, X. Yang, S. Gao and R. Cao, *Catal. Sci. Technol.*, 2018, **8**, 1288–1295.
34 D. Chen, H. Xing, C. Wang and Z. Su, *J. Mater. Chem. A*, 2016, **4**, 2657–2662.
35 N. Sadeghi, S. Sharifnia and T. Do, *J. Mater. Chem. A*, 2018, **6**, 18031–18035.
36 Z. Jiang, X. Xu, Y. Ma, H. S. Cho, D. Ding, C. Wang, J. Wu, P. Oleynikov, M. Jia, J. Cheng, Y. Zhou, O. Terasaki, T. Peng, L. Zan and H. Deng, *Nature*, 2020, **586**, 549–554.
37 H. Tsuneoka, K. Teramura, T. Shishido and T. Tanaka, *J. Phys. Chem. C*, 2010, **114**, 8892–8898.
38 Y. Wang, Q. Xia, X. Bai, Z. Ge, Q. Yang, C. Yin, S. Kang, M. Dong and X. Li, *Appl. Catal., B*, 2018, **239**, 196–203.
39 T. W. Woolerton, S. Sheard, E. Pierce, S. W. Ragsdale and F. A. Armstrong, *Energy Environ. Sci.*, 2011, **4**, 2393.
40 Y. Wang, J. Liu, Y. Wang and M. Zhang, *RSC Adv.*, 2020, **10**, 8821–8824.
41 C. Yuan, Y. He, R. Chen, Y. Sun, J. Li, W. Cui, P. Chen, J. Sheng and F. Dong, *Sol. RRL*, 2021, **5**, 1–16.
42 S. Shyamal and N. Pradhan, *J. Phys. Chem. Lett.*, 2020, **11**, 6921–6934.
43 H. Wang, X. Wang, H. Zhang, W. Ma, L. Wang and X. Zong, *Nano Energy*, 2020, **71**, 104647.
44 S. H. Guo, J. Zhou, X. Zhao, C. Y. Sun, S. Q. You, X. L. Wang and Z. M. Su, *J. Catal.*, 2019, **369**, 201–208.
45 C. Han, X. Zhu, J. S. Martin, Y. Lin, S. Spears and Y. Yan, *ChemSusChem*, 2020, **13**, 4005–4025.
46 K. Hong, Q. Van Le, S. Y. Kim and H. W. Jang, *J. Mater. Chem. C*, 2018, **6**, 2189–2209.
47 X. Wang, T. Zhang, Y. Lou and Y. Zhao, *Mater. Chem. Front.*, 2019, **3**, 365–375.
48 P. Zhang, J. Yang and S. H. Wei, *J. Mater. Chem. A*, 2018, **6**, 1809–1815.
49 M. Usman and Q. Yan, *Crystals*, 2020, **10**, 62.
50 X. Wang, J. He, J. Li, G. Lu, F. Dong, T. Majima and M. Zhu, *Appl. Catal., B*, 2020, **277**, 119230.
51 S. S. Bhosale, A. K. Kharade, E. Jokar, A. Fathi, S. M. Chang and E. W. G. Diau, *J. Am. Chem. Soc.*, 2019, **141**, 20434–20442.
52 Q. A. Akkerman, G. Rainò, M. V. Kovalenko and L. Manna, *Nat. Mater.*, 2018, **17**, 394–405.
53 M. V. Kovalenko, L. Protesescu and M. I. Bodnarchuk, *Science*, 2017, **358**, 745–750.
54 J. Wang, J. Liu, Z. Du and Z. Li, *J. Energy Chem.*, 2021, **54**, 770–785.
55 H. Huang, B. Pradhan, J. Hofkens, M. B. J. Roeffaers and J. A. Steele, *ACS Energy Lett.*, 2020, **5**, 1107–1123.
56 M. Muringa Kandy, A. Rajeev K and M. Sankaralingam, *Sustainable Energy Fuels*, 2021, **15**, 12–33.
57 J. Mao, K. Li and T. Peng, *Catal. Sci. Technol.*, 2013, **3**, 2481.
58 J. Hong, W. Zhang, J. Ren and R. Xu, *Anal. Methods*, 2013, **5**, 1086.
59 S. Protti, A. Albini and N. Serpone, *Phys. Chem. Chem. Phys.*, 2014, **16**, 19790–19827.
60 W. A. Thompson, E. Sanchez Fernandez and M. M. Maroto-Valer, *ACS Sustainable Chem. Eng.*, 2020, **8**, 4677–4692.
61 X. Chang, T. Wang and J. Gong, *Energy Environ. Sci.*, 2016, **9**, 2177–2196.
62 M. A. Green, A. Ho-Baillie and H. J. Snaith, *Nat. Photonics*, 2014, **8**, 506–514.
63 B. Saparov and D. B. Mitzi, *Chem. Rev.*, 2016, **116**, 4558–4596.
64 M. Ahmadi, T. Wu and B. Hu, *Adv. Mater.*, 2017, **29**, 1–24.
65 J. Deng, J. Li, Z. Yang and M. Wang, *J. Mater. Chem. C*, 2019, **7**, 12415–12440.
66 J. Hou, S. Cao, Y. Wu, Z. Gao, F. Liang, Y. Sun, Z. Lin and L. Sun, *Chem. – Eur. J.*, 2017, **23**, 9481–9485.
67 C. Tang, C. Chen, W. Xu and L. Xu, *J. Mater. Chem. A*, 2019, **7**, 6911–6919.
68 S. Shyamal, S. K. Dutta, T. Das, S. Sen, S. Chakraborty and N. Pradhan, *J. Phys. Chem. Lett.*, 2020, **11**, 3608–3614.
69 Y.-W. Liu, S.-H. Guo, S.-Q. You, C.-Y. Sun, X.-L. Wang, L. Zhao and Z.-M. Su, *Nanotechnology*, 2020, **31**, 215605.
70 Q. Fan, G. V. Biesold-McGee, J. Ma, Q. Xu, S. Pan, J. Peng and Z. Lin, *Angew. Chem., Int. Ed.*, 2020, **59**, 1030–1046.
71 S. Khalfin and Y. Bekenstein, *Nanoscale*, 2019, **11**, 8665–8679.
72 L. Zhou, Y. F. Xu, B. X. Chen, D. Bin Kuang and C. Y. Su, *Small*, 2018, **14**, 1703762.
73 E. M. Hutter, M. C. Gélvez-Rueda, D. Bartesaghi, F. C. Grozema and T. J. Savenije, *ACS Omega*, 2018, **3**, 11655–11662.
74 S. Bhaumik, S. Ray and S. K. Batabyal, *Mater. Today Chem.*, 2020, **18**, 100363.
75 C. Lu, D. S. Itanze, A. G. Aragon, X. Ma, H. Li, K. B. Ucer, C. Hewitt, D. L. Carroll, R. T. Williams, Y. Qiu and S. M. Geyer, *Nanoscale*, 2020, **12**, 2987–2991.
76 J. Sheng, Y. He, J. Li, C. Yuan, H. Huang, S. Wang, Y. Sun, Z. Wang and F. Dong, *ACS Nano*, 2020, **14**, 13103–13114.
77 Z. C. Kong, J. F. Liao, Y. J. Dong, Y. F. Xu, H. Y. Chen, D. Bin Kuang and C. Y. Su, *ACS Energy Lett.*, 2018, **3**, 2656–2662.
78 Y. Jiang, J. F. Liao, H. Y. Chen, H. H. Zhang, J. Y. Li, X. D. Wang and D. Bin Kuang, *Chem*, 2020, **6**, 766–780.
79 Y. Jiang, J.-F. Liao, Y.-F. Xu, H.-Y. Chen, X.-D. Wang and D.-B. Kuang, *J. Mater. Chem. A*, 2019, **7**, 13762–13769.
80 H. Wang, L. Zhang, Z. Chen, J. Hu, S. Li, Z. Wang, J. Liu and X. Wang, *Chem. Soc. Rev.*, 2014, **43**, 5234.
81 X. D. Wang, Y. H. Huang, J. F. Liao, Y. Jiang, L. Zhou, X. Y. Zhang, H. Y. Chen and D. Bin Kuang, *J. Am. Chem. Soc.*, 2019, **141**, 13434–13441.
82 R. Cheng, H. Jin, M. B. J. Roeffaers, J. Hofkens and E. Debroye, *ACS Omega*, 2020, **5**, 24495–24503.

83 M. Ou, W. Tu, S. Yin, W. Xing, S. Wu, H. Wang, S. Wan, Q. Zhong and R. Xu, *Angew. Chem.*, 2018, **130**, 13758–13762.
84 J. Wang, J. Wang, N. Li, X. Du, J. Ma, C. He and Z. Li, *ACS Appl. Mater. Interfaces*, 2020, **12**, 31477–31485.
85 S. Wan, M. Ou, Q. Zhong and X. Wang, *Chem. Eng. J.*, 2019, **358**, 1287–1295.
86 J. Meng, Q. Chen, J. Lu and H. Liu, *ACS Appl. Mater. Interfaces*, 2019, **11**, 550–562.
87 L. Wu, Y. Mu, X. Guo, W. Zhang, Z. Zhang, M. Zhang and T. Lu, *Angew. Chem., Int. Ed.*, 2019, **58**, 9491–9495.
88 R. Cheng, E. Debroye, J. Hofkens and M. B. J. Roeffaers, *Catalysts*, 2020, **10**, 1352.
89 Q. Wang, J. Wang, J. C. Wang, X. Hu, Y. Bai, X. Zhong and Z. Li, *ChemSusChem*, 2021, **230026**, 1131–1139.
90 Y. F. Mu, W. Zhang, X. X. Guo, G. X. Dong, M. Zhang and T. B. Lu, *ChemSusChem*, 2019, **12**, 4769–4774.
91 G. X. Dong, W. Zhang, Y. F. Mu, K. Su, M. Zhang and T. B. Lu, *Chem. Commun.*, 2020, **56**, 4664–4667.
92 X. Wang, J. He, L. Mao, X. Cai, C. Sun and M. Zhu, *Chem. Eng. J.*, 2020, 128077.
93 X. Guo, S. Tang, Y. Mu, L. Wu, G. Dong and M. Zhang, *RSC Adv.*, 2019, **9**, 34342–34348.
94 P. Li, Y. Zhou, H. Li, Q. Xu, X. Meng, X. Wang, M. Xiao and Z. Zou, *Chem. Commun.*, 2015, **51**, 800–803.
95 J. Jin, J. Yu, D. Guo, C. Cui and W. Ho, *Small*, 2015, **11**, 5262–5271.
96 Y. Wei, J. Jiao, Z. Zhao, W. Zhong, J. Li, J. Liu, G. Jiang and A. Duan, *J. Mater. Chem. A*, 2015, **3**, 11074–11085.
97 Y. Mu, W. Zhang, G. Dong, K. Su, M. Zhang and T. Lu, *Small*, 2020, **16**, 2002140.
98 F. Xu, K. Meng, B. Cheng, S. Wang, J. Xu and J. Yu, *Nat. Commun.*, 2020, **11**, 4613.
99 X. Li, J. Yu, M. Jaroniec and X. Chen, *Chem. Rev.*, 2019, **119**, 3962–4179.
100 J.-F. Liao, Y.-T. Cai, J.-Y. Li, Y. Jiang, X.-D. Wang, H.-Y. Chen and D.-B. Kuang, *J. Energy Chem.*, 2021, **53**, 309–315.
101 A. Pan, X. Ma, S. Huang, Y. Wu, M. Jia, Y. Shi, Y. Liu, P. Wangyang, L. He and Y. Liu, *J. Phys. Chem. Lett.*, 2019, **10**, 6590–6597.
102 Z. Chen, Y. Hu, J. Wang, Q. Shen, Y. Zhang, C. Ding, Y. Bai, G. Jiang, Z. Li and N. Gaponik, *Chem. Mater.*, 2020, **32**, 1517–1525.
103 Y.-F. Xu, M.-Z. Yang, H.-Y. Chen, J.-F. Liao, X.-D. Wang and D.-B. Kuang, *ACS Appl. Energy Mater.*, 2018, **1**, 5083–5089.
104 Y.-X. Chen, Y.-F. Xu, X.-D. Wang, H.-Y. Chen and D.-B. Kuang, *Sustainable Energy Fuels*, 2020, **4**, 2249–2255.
105 A. K. Jena, A. Kulkarni and T. Miyasaka, *Chem. Rev.*, 2019, **119**, 3036–3103.
106 J. Z. Y. Tan and M. M. Maroto-Valer, *J. Mater. Chem. A*, 2019, **7**, 9368–9385.